Turkish Journal of Science & Technology
19(1), 237-247, 2024

Research Paper
https://doi.org/10.55525/tjst.1401275

Effect of Ferro-Alloys on the Properties of High Entropy Alloy with FeCoNiMnMoV Composition Produced by Arc-Melting Method

Seval Hale GÜLER[1*]
[1] Rare Earth Elements Application and Research Center, Munzur University 62000, Tunceli, Türkiye
[*1]sevalhaleguler@munzur.edu.tr

(Geliş/Received: 07/12/2023; Kabul/Accepted: 26/02/2024)

Abstract: In this study, high entropy FeCoNiMnMoV and FeCoNiMn (Ferro Mo-Ferro-V) alloys were produced by arc melting method. After the arc melting process, the samples were annealed at 1000°C under argon atmosphere for 15 hours physical and thermodynamic calculations were performed to determine the properties of the alloy. In the study, both alloys were characterized. For characterization, XRD, SEM, EDS and Micro hardness were taken from the samples. The aim of my study is to examine the effect of using low-priced starting materials on the microstructure of HEA. For this purpose, ferro-alloys were added to the alloy. As a result, similar properties were obtained for the microstructure of both alloys. However, it has been determined that the hardness of samples containing ferro-alloys decreases more due to their chemical composition, especially after heat treatment.

Key words: High Entropy Alloy, Arc Melting, Ferro Alloys, SEM, Hardness.

Ark-Ergitme Yöntemi ile Üretilen FeCoNiMnMoV Bileşimine Sahip Yüksek Entropili Alaşımın Özelliklerine Ferro-Alaşımların Etkisi

Öz: Bu çalışmada yüksek entropili FeCoNiMnMoV ve FeCoNiMn (Ferro Mo-Ferro V) alaşımları ark ergitme yöntemi ile üretilmiştir.Ark ergitme işlemi sonrası numenelere 1000°C'de argon atmosferi altında 15 saat tavlama işlemi uygulanmıştır. Alaşımın özelliklerini belirlemek için fiziksel ve termodinamik hesaplamalar yapılmıştır. Çalışmada her iki alaşım karakterize edilmiştir. Karakterizasyon için numunelerden XRD, SEM,EDS,Mikro sertlik alınmıştır. Çalışmanım amacı düşük fiyatlı başlangıç malzemelerinin kullanılmasının HEA'ların mikro yapısına etkisini incelemektir. Bu amaçla alaşımın içine ferro alaşımlar ilave edilmiştir. Sonuç olarak, her iki alaşım mikro yapısı için benzer özellikler elde edilmiştir. Ancak özellikle ısıl işlemden sonra ferro alaşımlı numunelerin kimyasal bileşimlerinden kaynaklı olarak sertliklerinin daha fazla düştüğü tespit edilmiştir.

Anahtar Kelimeler: Yüksek Entropili Alaşım, Ark Ergitme, Ferro Alaşımlar, SEM, Sertlik.

Introduction

Some properties are improved and some are worsened by the alloy. The intermetallics that are hard and brittle and form in the structure make the alloy stronger, but they also make it less plastic[1]. Each new material leads to a new application area, thus leading to the development of engineering practices. The search for new materials continues at full speed today. In many traditional alloys, a family of alloys based on the main element is obtained by adding different types of alloying elements to a main element [2]. For example, Zn, Mg, Si, Mn added to Al causes the emergence of new alloys with different properties. While Si provides increased strength, Mg causes the development of corrosion properties. [3]. The formation of complex microstructures, intermetallic compounds and precipitate phases is the result of adding different metals to the base metal in various proportion [4]. Intermetallic compounds that are typically hard and brittle are formed when the amount of minor alloy element increases. The strength of the alloys is enhanced, but the plasticity of the alloys frequently declines. [5]. In the alloy concept first proposed by YEH and her colleagues in 1995, new generation alloys that are not similar to traditional alloys have emerged [6] . This new generation alloy concept is called "high entropy alloy (HEA)". HEAs are groups of alloys containing 5 or more major elements [7, 8]. Each major element has a concentration between 5% and 35% [9, 10]. The mixing entropy in these alloys is very high compared to conventional alloys. Unlike conventional alloys, the formation of simple structured solid solution phases is observed in these alloys instead of several dozen phases and intermetallics that cause embrittlement. These simple structured solid solutions in HEAs make HEAs different from other alloys. High strength, excellent wear resistance, unusual fatigue resistance, low temperature strength, good corrosion resistance, antioxidation and excellent microstructural stability are the properties that make HEAs better than conventional alloys [11-14]. HEAs have the potential to be used in many engineering applications thanks to the unique properties they exhibit. HEAs have some disadvantages. One of them is their weight. The other is their cost, which is more important than their weight. Since HEAs are alloys obtained by adding at least 5

* Corresponding author: sevalhaleguler@munzur.edu.tr. ORCID Number of authors: 0000-0001-5888-9437

metals in equimolar and/or near-equimolar ratios, this causes their costs to increase [15]. The Ferro-alloy form of a metal is preferred over its pure form for alloying in the traditional alloy production sector. The reason is that the Ferro-alloy form of a metal is significantly less expensive than its pure form [16, 17]. The production of HEAs will be more affordable by using ferroalloys in HEAs. Ferroalloys are of two types; these are those produced in high quality and those produced in lower quality. Even in high quality Ferroalloys, there are still some impurities. The effect of these impurities found in ferroalloys on the properties of HEAs is an issue that needs to be investigated. In this study, HEA alloy in FeCoNiMnMoV composition was also produced using some Ferroalloys and the changes between the structural and some mechanical properties of both alloys were revealed.

2. Experimental Procedure

High purity V (Merck, 99.5%), Co (Merck, 99+%), Fe (Merck, 99%), Ni (Merck, 99.5%), Mo (Merck, 99.5%), Mn (Nanography, 99.5%) metals were used in the first method, and high purity Al, Co, Fe, Ni were used in the second method to produce HEA with FeCoNiMnMoV composition in this study. However, instead of high purity Mo and V, high quality Ferrovanadium and Ferromolybdenum were used. Ferrovanadium and Ferromolybdenum were obtained from Acarer Metal company and their compositions are given in Table 1.

Table 1. Compositions of Ferroalloys used in the study

Ferrovanadium		Ferromolybdenum	
V	65 % min	Mo	70 % min
Al	1.5 % max	Cu	0.5 % max
Si	2 % max	Si	1.5 % max
P	0.1 % max	S	0.01 % max
C	0.25 % max	C	0.1 % max
		P	0.05 % max

Table 2. Sample codes, composition, processes

Sample Code	Composition	Treatment
S1 (As-Cast)	Only Elemental Metal Powders	Arc Melting
S2 (As-Cast)	Ferroalloys and Elemental Metal Powders	Arc Melting
SG1 (Cast-Annealing)	Only Elemental Metal Powders	Annealing after Arc Melting
SG2 (Cast-Annealing)	Ferroalloys and Elemental Metal Powders	Annealing after Arc Melting

Sample codes and the procedures performed on the samples are given in Table 2. The powders weighed in appropriate proportions were mixed and turned into pellets. Then, the obtained pellets were melted 3 times consecutively using Arc-melting to obtain alloys. The other group of samples were subjected to annealing at 1000°C under argon atmosphere for 15 hours after the arc melting process (Table 2). The flow chart for the experiment is given in Figure 1.

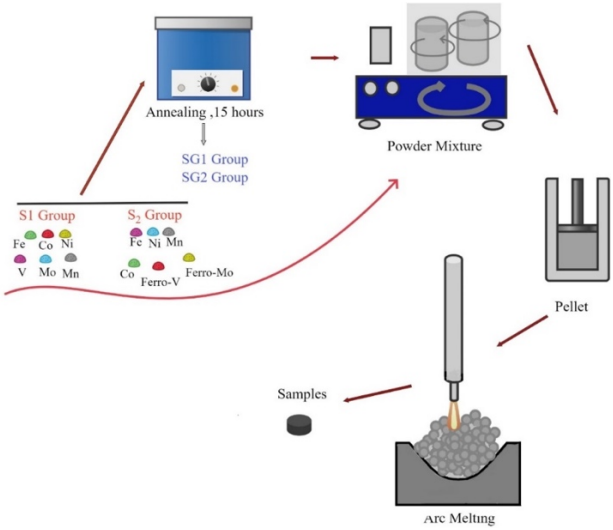

Figure 1. Experiment flow chart

The obtained samples were subjected to X-ray diffraction spectra (XRD, RIGAKU Miniflex 600) analysis for morphological examinations. Then, the samples were examined with scanning electron microscopes (SEM, Hitachi SU3500) and energy dispersive spectroscopy (EDX, Oxford AZtech) and Mitutoyo Corporation brand microhardness tester. Additionally, formulas for determining the properties of alloys are given in Table 3.

Table 3. Formulas required for physical and thermodynamic calculations of alloys

	Formulation	Amorphous	Solid solution (SS)	SS+Intermetalic (IM)
δ	$\delta = \sqrt{\sum C_i \left(\frac{1-r_i}{r}\right)^2}$ [18]	δ≥9 [19]	0≤ δ ≤8.5 [19]	SS and IM 3.6% ≤ δr < 6.6% IM ,δr ≥ 6.6 % [20]
Ω	$\Omega = \frac{T_m \, \Delta S_{mix}}{\lvert \Delta H_{mix} \rvert}$ [18]	-	Ω ≥1.1 [18]	IM 1 ≤ Ω ≤ 2 SS and IM 1.1 ≤ Ω ≤ 10 [20]
VEC	$VEC = \sum_i^n C_i \, (VEC)_i$ [21]	-	VEC ≤6.87 BCC VEC ≥ 8 FCC 6.87 ≤VEC ≥8: FCC+BCC [22]	-
ΔS_{mix}	$\Delta S_{mix} = -R \sum_i^n C_i \ln C_i$ [21]	7≤ ΔS_{mix} ≤14 Jmol^{-1} K^{-1} [19]	11≤ ΔS_{mix} ≤19.5 Jmol^{-1} K^{-1} [19]	-
ΔH_{Mix}	$\Delta H_{mix} = \sum_{i=1 \; j \neq i}^{n} 4\Delta H_{ij}^{mix}$ [21]	-35≤ ΔH_{mix} ≤-8.5 kJmol^{-1}[19]	-22≤ ΔH_{mix} ≤7 kJmol^{-1}[19]	Containg IM; ΔH_{mix} < -7.5 [20]

In the given equations, the value of n represents the number of components (ci and cj). i and j give the mole fractions of the elements in the alloy. In addition, the binary mixing enthalpy values (ΔHij_{mix}) between the elements i and j can be calculated with the Miedema approach [23].ΔS_{mix}, represents the mixture entropy, ΔS_{conf} represents the configuration entropy. δ gives the atomic size difference. In the formula (r) refers to the atomic diameter of the alloying elements. The term Ω refers to the probability of forming a solid solution. In this expression Ω, is a symbol of the conflict between entropy and enthalpy. VEC describes the valence electron configuration. Using the formulas in Table 3 and the Miedema approach, the thermodynamic and physical properties for the S1 and S2 alloy are given in Table 4.

Table 4. Physical and thermodynamic properties for samples S1 and S2

Sample Code	**ΔS_{conf}**	**ΔS_{mix}**	**ΔH_{Mix}**	**VEC**	**Ω**	**δ**	**T_m**
S1	1.79R	14.88	-4.377	7.47	6.07	7.28	1990.9
S2	1.77R	14.71	-2.91	7.55	9.92	7.36	1961.7

3. Results and Discussion

Figure 2 shows the XRD analysis results of samples S1, S2, SG1 and SG2. S1 sample is the sample produced using elemental metal powders and arc melting. Sample S2 is an HEA sample produced by arc melting using both elemental powders and ferro-alloys. 3 characteristic peaks are seen in both the XRD spectra of the S1 sample and the S2 sample (Figure 2.a - b). The most intense and broad peak at approximately 43^{o} is the peak showing BCC and FCC structure. Since the peak is strong and broad, the (111) FCC peak and the (110) BCC peak are on top.

Other characteristic peaks are the FCC peak at approximately 52° (200). The peak at approximately 73° is the (220) FCC peak.

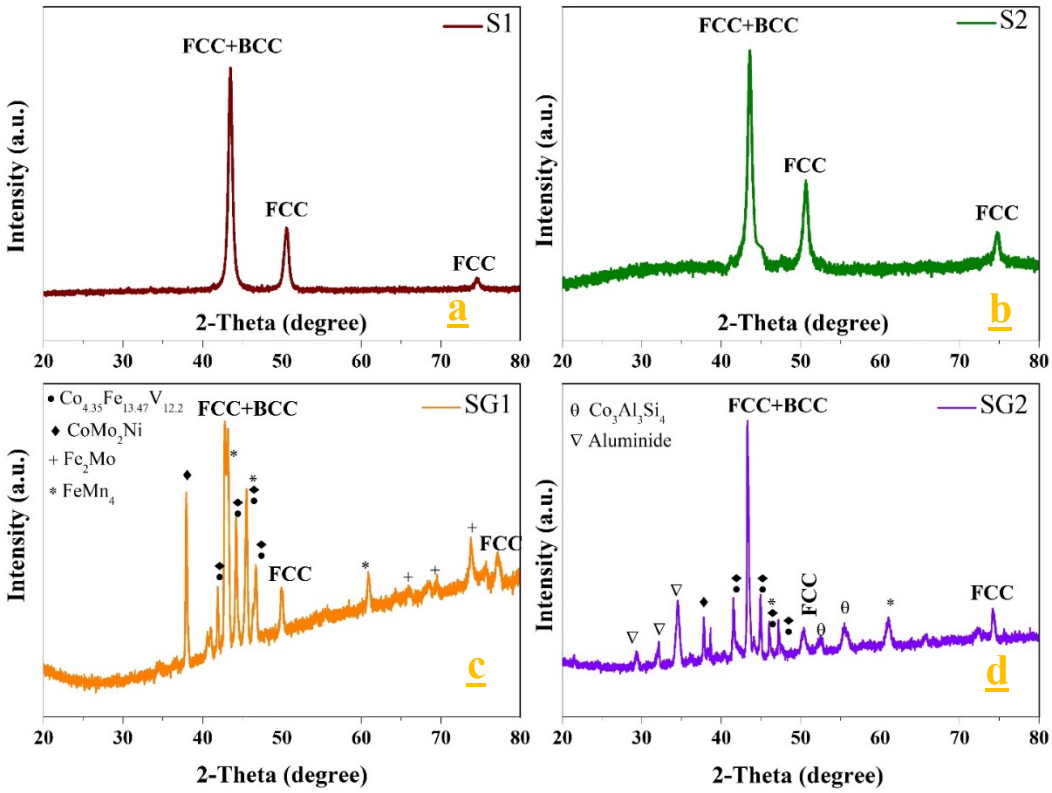

Figure 2. XRD spectra a) S1, b) S2, c) SG1, d) SG2

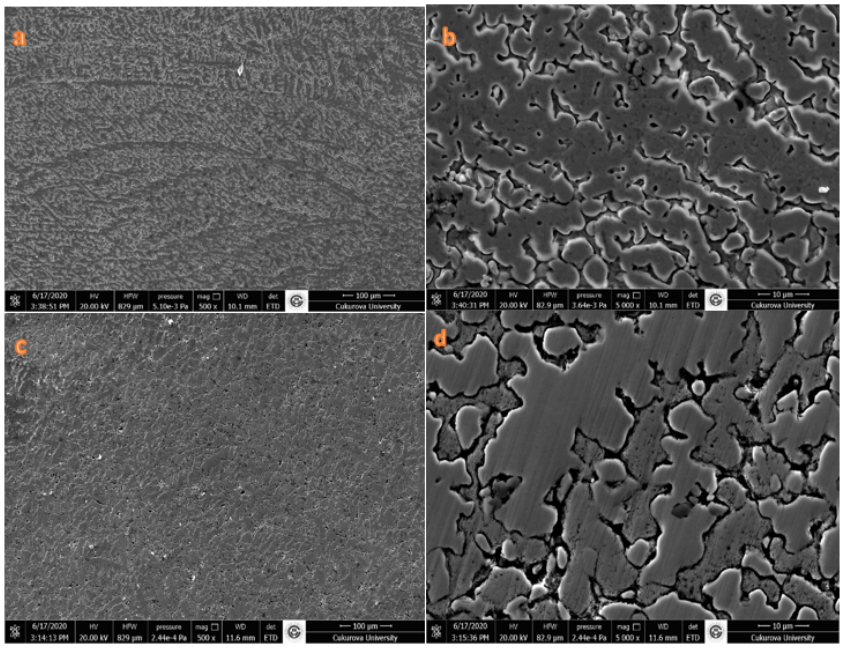

Figure 3. a) S1 (500X), b) S1 (5000X), c) S2 (500X), d) S2 (5000X)

XRD spectra of SG1 and SG2 samples are given in Figure 2c and d. SG1 and SG2 samples are the samples of S1 and S2 annealed at 1000°C for 15 hours after arc melting. As can be seen from the XRD spectra, the characteristic peaks at 43°, 52° and 73° are also present in the SG1 and SG2 samples. However, at the end of the annealing process, it is seen that $Co_{4.35}Fe_{13.47}$ $V_{12.2}$, $CoMo_2Ni$, Fe_2Mo and $FeMn_4$ structures precipitate. Additionally, $Co_3Al_3Si_4$ and various aluminides are observed to precipitate in the SG2 sample. The high annealing temperature of 1000 °C and the long annealing time of 15 hours caused the precipitation of such structures. Because both temperature and time contributed to the diffusion conditions for the formation of these structures. The main reason why these phases cannot precipitate in S1 and S2 samples is that cooling occurs very quickly after the arc melting process and there is not enough time for the metals in solid solution to come out of the cage. Therefore, solid solutions seen in classical HEAs were observed in samples S1 and S2. Although there is no Al and Si in the composition of the alloy, it was observed that $Co_3Al_3Si_4$ and various aluminides were formed in the SG2 sample. The reason for this situation is due to the ferro-alloys used in the SG2 sample. As seen in Table 1, Ferro-alloys contain up to 1.5% Al and Si.

Figure 3 shows the SEM images of S1 (Figure 3.a-b) and S2 (Figure 3.c-d) samples at different magnifications after casting. It is seen that the S1 sample has a thinner casting structure than the S2 sample and the dendritic structure is longer and more continuous. It is seen that the dendritic structure in the S2 sample is discontinuous and the grains are coarser compared to the S1 sample.

Each sample was inspected and analysed by scanning electron microscopy (SEM) and energy-dispersive X-ray spectroscopy (EDS), and mapping was carried out to verify the spatial distribution of the alloy components. A SEM image and typical mapping of a 6-component alloy is shown in Figure 4.(a-b). The regions in the mapping with a good distribution of alloying elements showed the formation of the high-entropy alloys that were the objective of this study. From these results, when the elemental mapping given in Figure.4 for the S1 sample of the microstructure of this alloy is examined, it is seen that Mo, V, Co, Fe elements are concentrated in the dendritic phase, while Ni and Mn are in the dendritic phase in less density. The mapping for each element is shown in the Figure.4 (c-h). It is seen that the regions rich in vanadium element are concentrated as a separate phase within this dendrite phase. In the interdendritic structure, Mn, Fe, Ni, Co elements are predominantly seen. V is not seen in the interdendritic structure.

In Figure 5.(a-b),SEM image and the elemental mapping for the sample S2 is given. The mapping for each element is shown in the Figure.5 (c-h). Here, similar to the S1 sample, it is seen that Mo, V are more concentrated in the dendritic phase, Mn and Ni elements are more concentrated between the dendrites, and Co and Fe are concentrated in both regions.

Figure 6 shows the microstructure images of SG1 (Figure 6.a-b) and SG2 (Figure 6.c-d) samples at different magnifications. SG1 and SG2 samples are the samples after heat treatment. Therefore, especially in the SG1 sample, it is seen that the dendritic arms in the structure have transformed into equiaxed grains. The structure is coarser in the SG2 sample. This suggests that the different elements in the ferro alloy cause a slow diffusion effect in the homogenization annealing.

Figure 7. (a-b) shows SEM image and the elemental distribution mapping for the SG1 sample. The mapping for each element is shown in the Figure.7 (c-h). With the effect of heat treatment, the elements are distributed more homogeneously between grains and grains. We can say that only Mo is present in the grain and the other elements are more homogeneously distributed. According to the XRD analysis given in Figure 2, different precipitates formed in the structure due to the effect of heat treatment. These precipitates are $Co_{4.35}Fe_{13.47}$ $V_{12.2}$, $CoMo_2Ni$, Fe_2Mo and $FeMn_4$

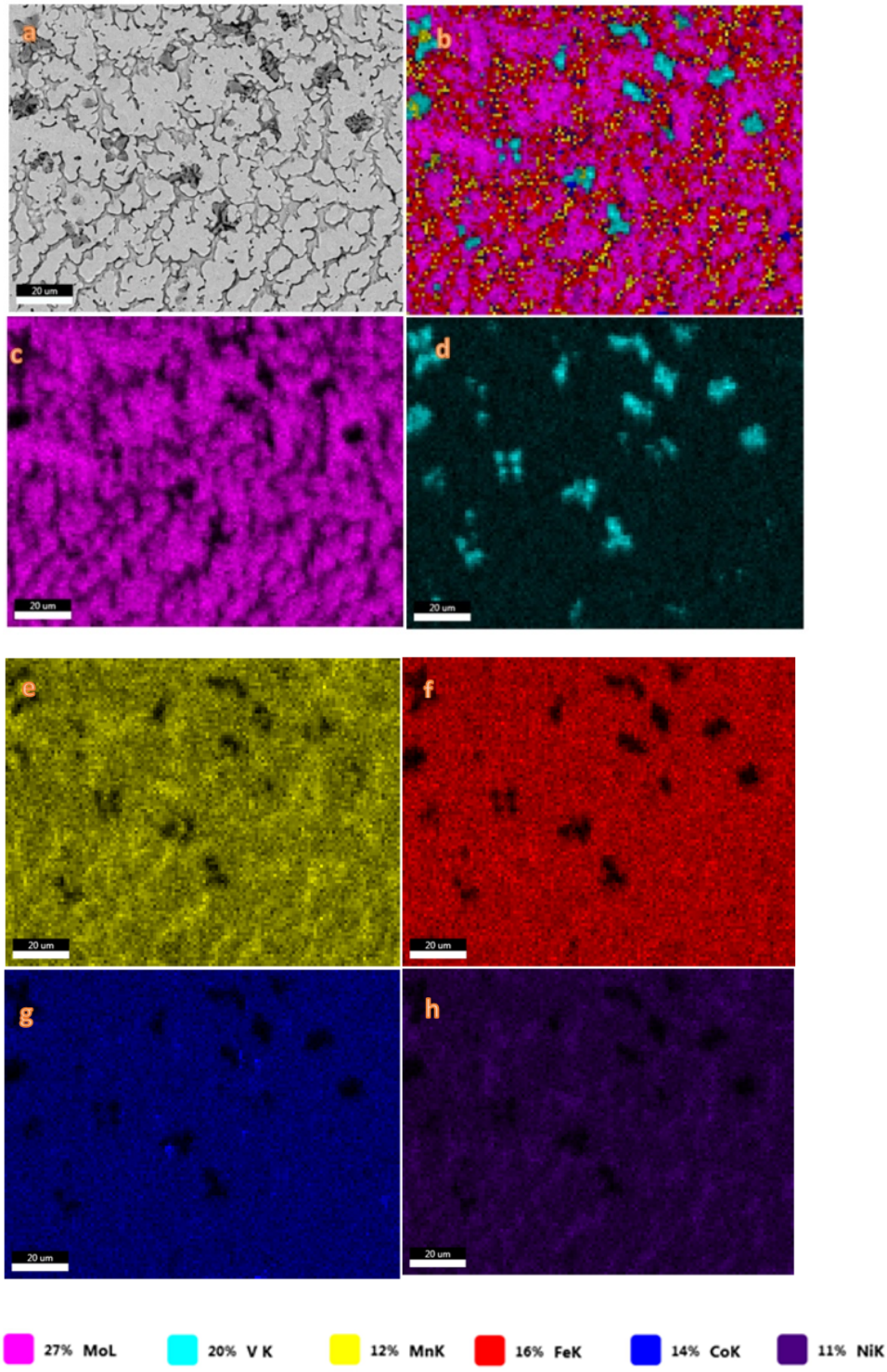

Figure 4. S1 sample a)SEM image b)Elemental distribution mapping for the sample c-h) The mapping for each element

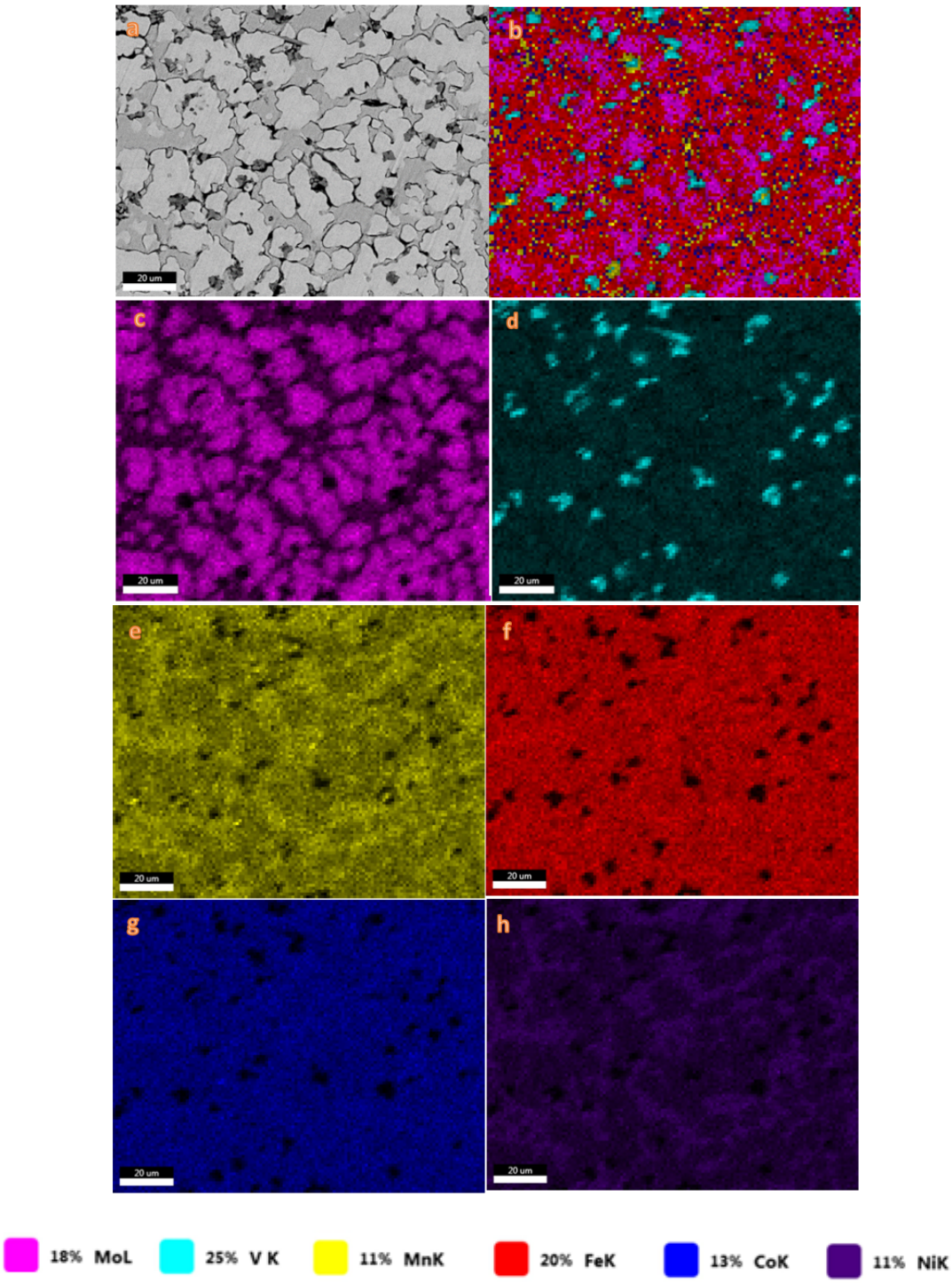

Figure 5. S2 sample a) SEM image b) Elemental distribution mapping for the sample c-h) The mapping for each element

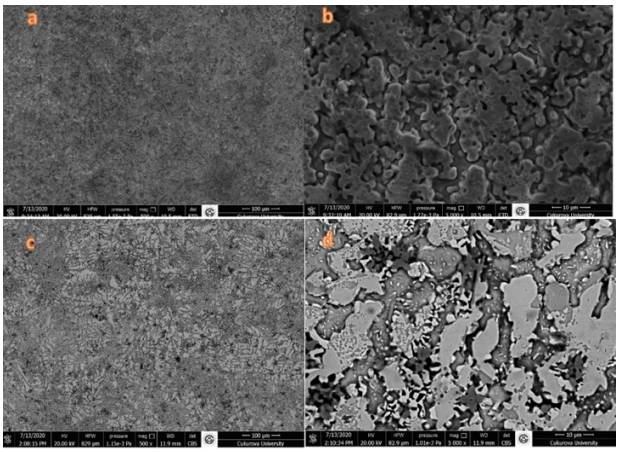

Figure 6. a) SG1 (500X), b) SG1 (5000X), c) SG2 (500X), d) SG2 (5000X)

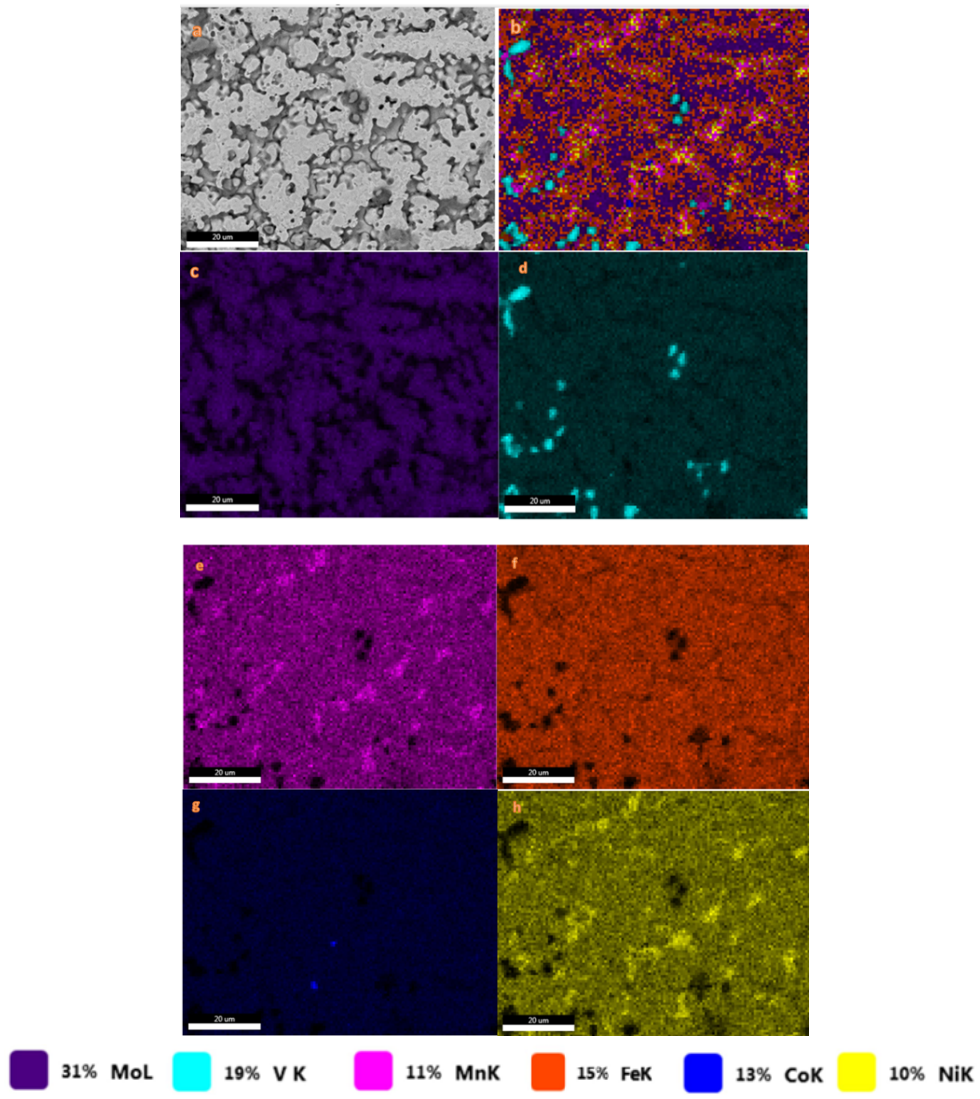

Figure 7. SG1 sample a) SEM image b)Elemental distribution mapping for the sample c-h) The mapping for each element

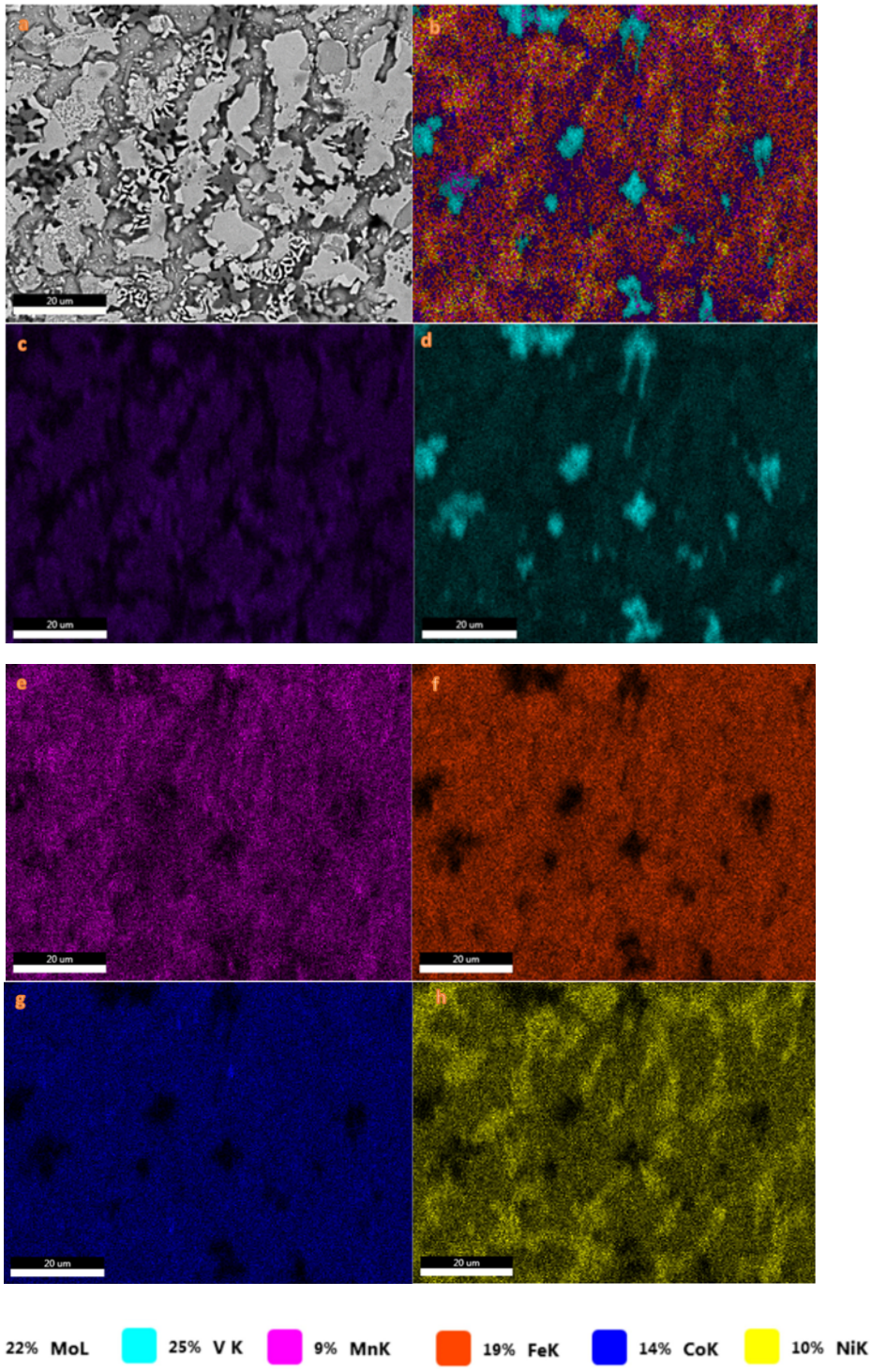

Figure 8. SG2 sample a) SEM image b)Elemental distribution mapping for the sample c-h) The mapping for each element

Figure 8. (a-b) shows the elemental distribution mapping and SEM image of the SG2 sample. The mapping for each element is shown in the Figure.8 (c-h). In Figure 8.a is seen that the regions rich in the V element have expanded. The Mo element is also present in the grain. Unlike SG1, Mn and Ni elements are concentrated at the grain boundary in the SG2 sample. According to the XRD graphs, $Co3Al_3Si_4$ and various aluminides were

precipitated for the SG2 sample. Although they are not included in the alloy, structures containing Al and Si come from ferroalloys.

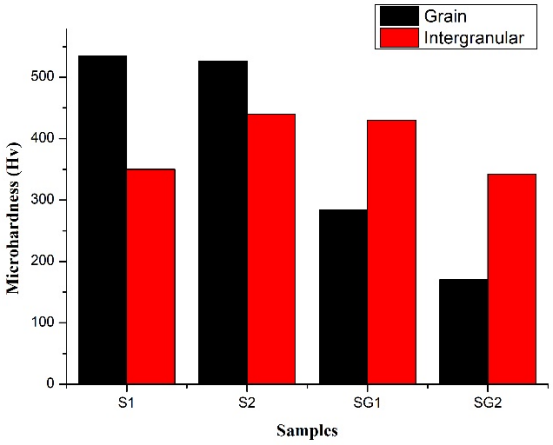

Figure 9. Microhardness of samples

In Figure 9, microhardness analysis was performed on the grain and intergranular regions of the samples. Accordingly, when S1 and SG1 samples were compared with each other, the hardness of the grain and intergranular region changed as a result of the separation and diffusion in the elements after the heat treatment. The same changes are observed in S2 and SG2 samples. Comparing S1 and S2, while the hardness within the grain does not change, the hardness in the intergranular region is higher than the S1 sample. In SG1 and SG2 samples, the effect of heat treatment is seen; while the hardness of the intragranular region decreases, an increase is observed in the intergranular region. This situation was considered as the expected effect of homogenization annealing. Because the elements had enough time to diffuse during annealing. The effect of lattice distortion provided by high entropy decreased with annealing. This caused a decrease in hardness.

4. Conclusions

This study focuses on investigating the effect of lower-priced starting materials to create high-entropy alloys. For this purpose, FeCoNiMnMoV and FeCoNiMn (Ferro Mo-Ferro-V) alloys have been successfully produced by the arc melting method. As a result of the microstructure research, a coarser grained structure was observed, especially in the samples with ferroalloy addition, after casting and after heat treatment. As a result of the microhardness test, it was observed that the hardness decrease was greater in ferro-alloy samples, especially after heat treatment.

References

[1] George EP, Raabe D, and Ritchie RO. High-entropy alloys. Nature reviews materials. 2019; 4:8: 515-534.
[2] Tsai M-H and Yeh J-W. High-entropy alloys: a critical review. Materials Research Letters. 2014; 2:3: 107-123.
[3] Rambabu P, Eswara Prasad N, Kutumbarao V, and Wanhill R. Aluminium alloys for aerospace applications. Aerospace materials and material technologies. 2017: 29-52.
[4] Shi Y, Collins L, Feng R, Zhang C, Balke N, Liaw PK, and Yang B. Homogenization of AlxCoCrFeNi high-entropy alloys with improved corrosion resistance. Corrosion Science. 2018; 133: 120-131.
[5] Xiao D, Zhou P, Wu W, Diao H, Gao M, Song M, and Liaw P. Microstructure, mechanical and corrosion behaviors of AlCoCuFeNi-(Cr, Ti) high entropy alloys. Materials & Design. 2017; 116: 438-447.
[6] Yeh JW, Chen SK, Lin SJ, Gan JY, Chin TS, Shun TT, Chang SY. Nanostructured high-entropy alloys with multiple principal elements: novel alloy design concepts and outcomes. Advanced engineering materials. 2004; 6:5: 299-303.
[7] Zhang Y, Zuo TT, Tang Z, Gao MC, Dahmen KA, Liaw PK, and Lu ZP. Microstructures and properties of high-entropy alloys. Progress in materials science. 2014; 61: 1-93.
[8] Murty BS, Yeh J-W, Ranganathan S, and Bhattacharjee P, High-entropy alloys. 2019: Elsevier.
[9] Santodonato LJ, Zhang Y, Feygenson M, Parish CM, Gao MC, Weber RJ, Liaw PK. Deviation from high-entropy configurations in the atomic distributions of a multi-principal-element alloy. Nature communications. 2015; 6:1: 1-13.

[10] Zhang Y, Yang X, and Liaw P. Alloy design and properties optimization of high-entropy alloys. Jom. 2012; 64:7: 830-838.
[11] Wu Z, Bei H, Pharr GM, and George EP. Temperature dependence of the mechanical properties of equiatomic solid solution alloys with face-centered cubic crystal structures. Acta Materialia. 2014; 81: 428-441.
[12] Verma A, Tarate P, Abhyankar A, Mohape M, Gowtam D, Deshmukh V, and Shanmugasundaram T. High temperature wear in CoCrFeNiCux high entropy alloys: The role of Cu. Scripta Materialia. 2019; 161: 28-31.
[13] George EP, Curtin W, and Tasan CC. High entropy alloys: A focused review of mechanical properties and deformation mechanisms. Acta Materialia. 2020; 188: 435-474.
[14] Shi Y, Yang B, and Liaw PK. Corrosion-resistant high-entropy alloys: A review. Metals. 2017; 7:2: 43.
[15] Fu X, Schuh CA, and Olivetti EA. Materials selection considerations for high entropy alloys. Scripta Materialia. 2017; 138: 145-150.
[16] Güler SH. The Effect of Using Ferro-Alloy on the Properties of AlCoFeNiMoTi High-Entropy Alloy Produced by Arc-Melting Method: Design of Low Cost. International Journal of Metalcasting. 2023: 1-10.
[17] Özkul İ. Characterization of AlCoCrFeNiVTi High Entropy Alloy Produced with Different Alloying Sources. Journal of Materials Engineering and Performance. 2023: 1-7.
[18] Youssef KM, Zaddach AJ, Niu C, Irving DL, and Koch CC. A novel low-density, high-hardness, high-entropy alloy with close-packed single-phase nanocrystalline structures. Materials Research Letters. 2015; 3:2: 95-99.
[19] Sheng G and Liu CT. Phase stability in high entropy alloys: Formation of solid-solution phase or amorphous phase. Progress in Natural Science: Materials International. 2011; 21:6: 433-446.
[20] Senkov O and Miracle D. A new thermodynamic parameter to predict formation of solid solution or intermetallic phases in high entropy alloys. Journal of Alloys and Compounds. 2016; 658: 603-607.
[21] Tian F, Varga LK, Chen N, Shen J, and Vitos L. Empirical design of single phase high-entropy alloys with high hardness. Intermetallics. 2015; 58: 1-6.
[22] Yang S, Lu J, Xing F, Zhang L, and Zhong Y. Revisit the VEC rule in high entropy alloys (HEAs) with high-throughput CALPHAD approach and its applications for material design-A case study with Al–Co–Cr–Fe–Ni system. Acta Materialia. 2020; 192: 11-19.
[23] Takeuchi A and Inoue A. Classification of bulk metallic glasses by atomic size difference, heat of mixing and period of constituent elements and its application to characterization of the main alloying element. Materials transactions. 2005; 46:12: 2817-2829.